

Design, Modeling, and Control of a Knee Exoskeleton for Underwater Load Assistance

Love Kumar Pathak¹, Harsh Mittal¹, Shiv Manjaree Gopaliya², Valayapathy Lakshmi Narayanan³ and Jyotindra Narayan^{1*}

¹Department of Mechanical Engineering, Indian Institute of Technology, Patna, Bihar, India

²School of Mechanical Engineering, VIT Bhopal University, Bhopal, India

³Department of Mechanical Engineering, Amrita Vishwa Vidyapeetham, Amritapuri, Kerala, India

Abstract. This study presents the design and control of a knee exoskeleton developed to assist humans while carrying loads through shallow or waist-level water. Conventional exoskeletons are designed for terrestrial applications and are inefficient in underwater conditions due to the effects of buoyancy, drag, and corrosion. To address this gap, an underwater knee exoskeleton is designed to augment strength while supporting a 51 kg load. The lightweight aluminium frame features adjustable lengths to accommodate users of varying anthropometric dimensions. To emulate the torque experienced at the knee joint during load-bearing, an existing knee joint kinematic dataset (angular motion and ground reaction force data) under aquatic conditions, corresponding to a 51 kg individual, is utilized in this work. A mathematical model was developed to estimate the torque requirements during the normal gait cycle, taking into account buoyant force and hydrodynamic drag. Thereafter, closed-loop position control was implemented using a PID controller in MATLAB Simscape Multibody, and its performance was analyzed for different gain combinations. Finally, numerical simulation results indicate that optimal PID gains achieved a mean absolute error of 4.05°, a root mean square error of 4.65°, and an integral absolute error of 4.07°. Moreover, a peak torque of 34.76 Nm is found to be necessary for the knee exoskeleton design to support additional loads of up to 51 kg in waist-level water. The results show that the proposed design and control strategy are effective for load augmentation in underwater conditions.

1 Introduction

In recent years, wearable devices such as exoskeletons have attracted significant attention for their potential to enhance human strength and reduce fatigue during walking. Lower limb exoskeletons are widely used in industrial, medical, and defense sectors to augment physical capability and reduce fatigue [1, 2]. Generally, exoskeletons are mainly divided into three categories: load augmentation exoskeletons, designed to increase load carrying capacity while minimizing fatigue and chances of injuries; rehabilitation exoskeletons, which assist patients in restoring mobility and muscular coordination during recovery from neuromuscular

*e-mail: jnarayan@iitp.ac.in

injuries [3, 4]; and assistive exoskeletons, which provide motion support to individuals with partial mobility limitations in daily activities [5].

The Berkeley Lower Extremity Exoskeleton (BLEEX) and Fontanan Full Body Extender are among the early full-body exoskeletons developed for industrial load-carrying applications [6, 7]. More recently, developments in load-augmentation exoskeletons have shown a variety of approaches for military and industrial use. For example, the HyExo is a quasi-passive hydraulic exoskeleton designed for load augmentation that exhibits a 7.8% reduction in the metabolic energy expenditure of wearers while carrying a 30 kg load [8]. Another recent development is a shank-free exoskeleton (without any physical connection with the human shank) that has five degrees of freedom (DOF) on each leg, three of which are powered by actuators, and shows a 10.94% reduction in metabolic energy expenditure while carrying a 27.1 kg load [9]. Similarly, affordable and adaptive full-body exoskeletons are also developed for industrial workers to prevent back injuries while carrying heavy loads [10]. In addition, an underwater lower-extremity soft exoskeleton is designed to assist swimmers during the breaststroke. This exoskeleton integrates an actuation system within a portable, waterproof cabin attached to the back of the swimsuit [11]. In the rehabilitation, the NOHA system integrates lower-limb exoskeletons with aquatic therapy principles for the recovery of individuals with neurological impairments [12]. While there has been progress in underwater exoskeletons for rehabilitation and swimming assistance, research focusing on load augmentation in underwater conditions remains largely unexplored.

Military personnel are often required to carry heavy loads on their backs, which is approximately 60% of their total body weight [13], through complex terrains, including shallow or waist-level water conditions, where drag and buoyancy significantly affect locomotion and load handling efficiency. Conventional exoskeletons are primarily developed for terrestrial applications and are not optimized for underwater conditions. This paper presents the comprehensive design, dynamic analysis, and PID-based control of a knee exoskeleton for underwater load augmentation. The specific novelty of this study lies in the development of a knee exoskeleton capable of effective load augmentation in an underwater environment, a research area that remains unexplored in existing exoskeleton studies. The proposed design uniquely addresses the effects of buoyancy, drag, and corrosion, enabling reliable load augmentation in shallow or waist-level water. The proposed design focuses on developing a lightweight, adjustable-length, and corrosion-resistant knee exoskeleton suitable for underwater applications. Control simulations were performed using Simulink Multibody to analyze the performance of PID control and to estimate the maximum knee joint torque for actuator selection. Additionally, a mathematical model has been developed to estimate knee joint torque during walking in waist-level water.

2 Design of Underwater Knee Exoskeleton

Knee exoskeleton consists of two links: a thigh frame and a shank frame, whose dimensions are based on anthropometric data for individuals aged between 25-30 years to ensure a proper fit and comfort [14]. Both frames feature adjustable lengths using a slider-hole locking mechanism, allowing accommodation of users with heights ranging from 160 cm to 180 cm. The thigh frame has three locking positions corresponding to lengths of 370 mm, 400 mm, and 420 mm, while the shank frame has three positions at 390 mm, 420 mm, and 440 mm. For the structural components, Aluminium alloy 6061-T6 was selected due to its high strength-to-weight ratio, good corrosion resistance, and excellent machinability [15]. The total weight of the exoskeleton frame (without the actuator) is 1.8 kg per leg. The knee exoskeleton was modeled in Autodesk Fusion 360, and the final design is shown in Figure 1.

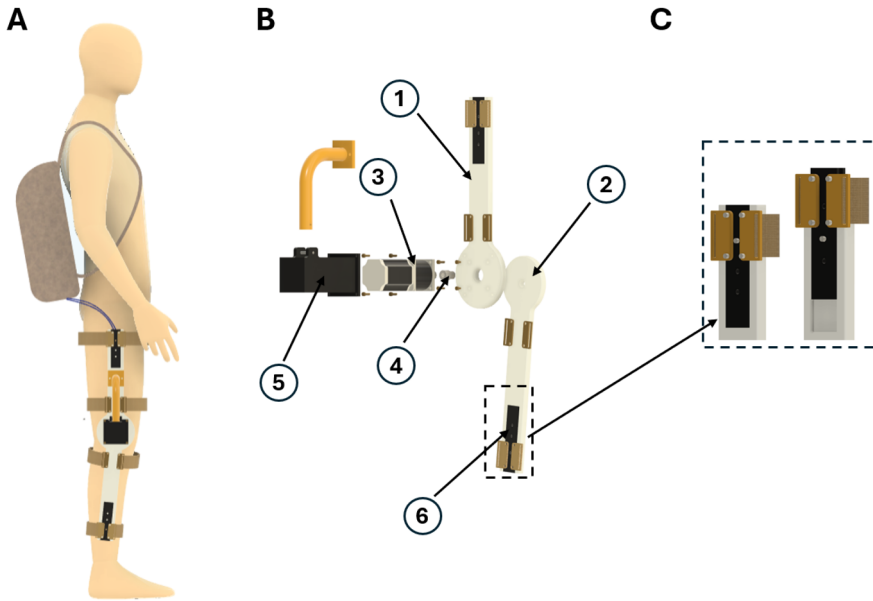


Figure 1. Design and components of the knee exoskeleton. (A) Knee exoskeleton with human model (B) Schematic of the exoskeleton linkages and actuator configuration: (1) thigh frame, (2) shank frame, (3) actuator, (4) coupler, (5) motor housing, and (6) Slider. (C) Adjustable slider-hole mechanism on the thigh and shank frames.

The knee exoskeleton is designed to provide assistive torque for carrying loads up to 51 kg while walking in waist-level water. While modeling the exoskeleton, existing joint kinematics and ground reaction force data corresponding to a 51 kg individual are utilized to simulate the joint torque demands under aquatic load-bearing conditions. The knee joint angles and ground reaction forces (GRFs) while walking in waist-level water are illustrated in Figure 2.

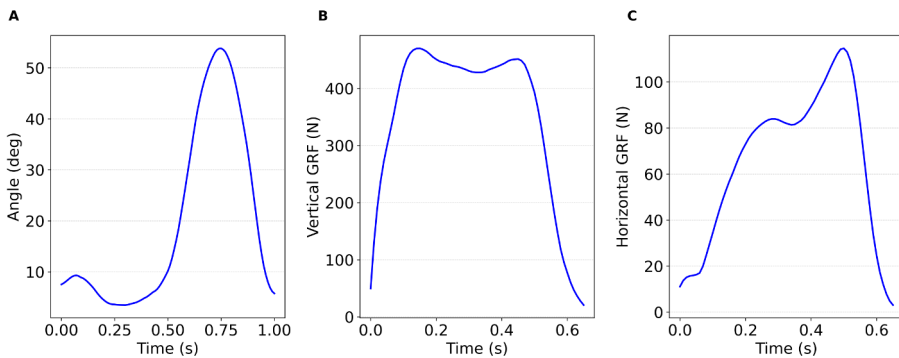


Figure 2. Knee joint kinematics over the complete gait cycle and ground reaction forces during the stance phase for a 51 kg individual walking in waist-deep water [16]: (A) knee joint angle, (B) vertical ground reaction force, and (C) horizontal ground reaction force.

3 Dynamics of Underwater Knee exoskeleton

The dynamic behavior of the knee exoskeleton during walking in waist-level water is analyzed to determine the peak torque required at the knee joint. The analysis considers a normal gait cycle, which is divided into stance and swing phases. During the stance phase, the foot maintains contact with the ground, and the ground reaction forces act on the foot, whereas in the swing phase, there is no contact between the foot and the ground. Since the walking speed in water is low (slow walking), inertial effects are neglected, and quasi-static conditions are assumed.

The exoskeleton and limb segment (shank) are modeled as rigid links with concentrated masses at their centers of mass. For a single leg, the knee joint torque τ_k is required to balance the moments due to multiple forces: the weight of the limb segments and frame, the buoyant force from water, the GRFs during stance, and the hydrodynamic drag torque [17, 18]. The free-body diagram of the shank and foot is shown in Figure 3.

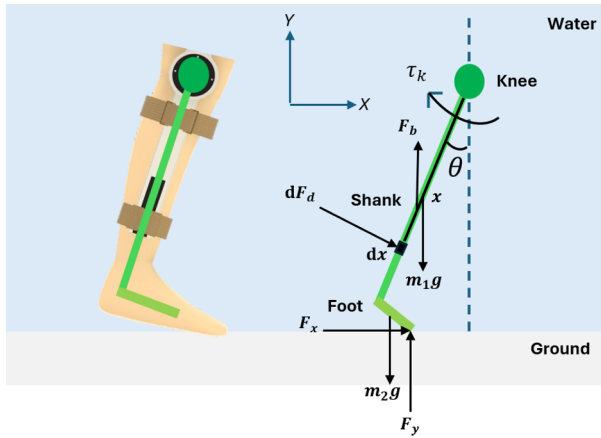


Figure 3. Free-body diagram of the shank and foot during the stance phase. m_1 represents the combined mass of the human shank and the exoskeleton frame, while m_2 denotes the mass of the foot. l is the length of the shank and frame, and F_x and F_y are the horizontal and vertical components of the ground reaction force, respectively.

Stance Phase:

$$\tau_k = m_1g \cdot \frac{l}{2} \cdot \sin \theta + m_2g \cdot l \cdot \sin \theta + F_x \cdot l \cdot \cos \theta - F_y \cdot l \cdot \sin \theta - F_b \cdot \frac{l}{2} \cdot \sin \theta + \tau_d \quad (1)$$

Swing Phase:

$$\tau_k = m_1g \cdot \frac{l}{2} \cdot \sin \theta + m_2g \cdot l \cdot \sin \theta - F_b \cdot \frac{l}{2} \cdot \sin \theta + \tau_d \quad (2)$$

Calculation of drag torque:

The shank is modeled as a straight cylinder of constant radius r for drag torque calculations. For an infinitesimal element of length dx , the drag force acting on this infinitesimal element is given as follows:

$$dF_d = -\frac{1}{2}\rho C_d v^2 dA \quad (3)$$

For a rotating shank, the local velocity at a distance x from the knee joint is $v = \omega x$, and the projected area perpendicular to the flow is $dA = 2r dx$. Therefore,

$$dF_d = -\frac{1}{2}\rho C_d(\omega x)^2(2r dx) \quad (4)$$

The elemental drag torque about the knee joint is then

$$d\tau_d = -\rho C_d r \omega^2 x^3 dx \quad (5)$$

On integrating, the total drag torque acting on the shank is obtained as

$$\tau_d = -\frac{1}{4}\rho C_d r \omega^2 \ell^4 \quad (6)$$

The negative sign indicates that the drag torque acts in a direction opposite to the direction of rotation.

Calculation of buoyant force:

The buoyant force acting on a shank and foot is given as:

$$F_b = V\rho_w g \quad (7)$$

$$F_b = \frac{\rho_w}{\rho} mg \quad (8)$$

where ρ_w is the density of water, ρ is the density of human tissue, and m denotes mass of the shank-foot.

4 Control Strategy for Underwater Knee exoskeleton

The simulation and control of the knee exoskeleton were performed using MATLAB Simscape Multibody. It is a physics-based simulation environment that allows modeling of mechanical systems without explicitly deriving complex dynamic equations. The software automatically computes the system dynamics based on the defined physical connections, joints, and constraints. The knee exoskeleton was designed in Fusion 360 and then imported into Onshape, a cloud-based CAD platform that provides the facility to directly export assemblies into Simscape Multibody. In Onshape, appropriate joints and constraints were defined to represent the kinematic behavior of the human leg-exoskeleton system. The finalized model was exported to Simscape Multibody for dynamic analysis and control simulation.

The tracking error is defined as

$$e(t) = \theta_d(t) - \hat{\theta}(t) \quad (9)$$

where θ_d is the desired knee angle and $\hat{\theta}$ is the measured joint angle from the revolute joint.

The control torque output of the PID controller is expressed as

$$u(t) = K_p e(t) + K_i \int_0^t e(\tau) d\tau + K_d \frac{de(t)}{dt} \quad (10)$$

where K_p , K_i , and K_d represent the proportional, integral, and derivative gains, respectively.

A PID control strategy was employed to track the desired knee joint trajectory. PID control is one of the most widely used and simple closed-loop control techniques for trajectory

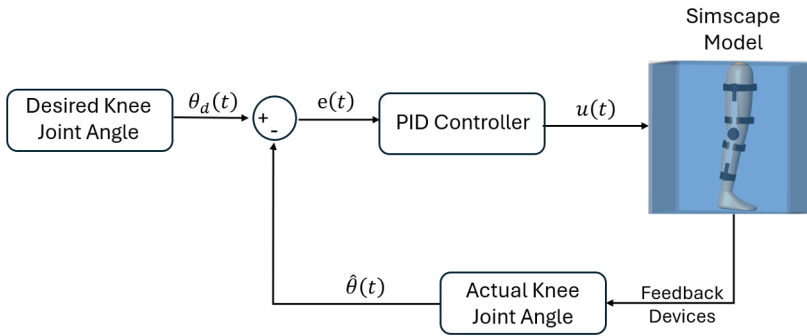


Figure 4. Schematic of the closed-loop control system for the leg exoskeleton.

tracking. The desired trajectory was provided as input to the controller, while the actual knee joint angle measured using the revolute joint block was provided as feedback for the closed-loop control. The overall control architecture is shown in Figure 4. To simulate underwater conditions, ground reaction forces, buoyant forces, and hydrodynamic drag torques were applied using External Force and Torque blocks in Simscape Multibody. The control signal generated by the PID controller depends on three gains: proportional gain (K_p), which accounts for the present error (difference between desired and actual knee joint trajectories) and provides a fast response; integral gain (K_i) which accumulate past errors to eliminate steady-state error; and derivative gain (K_d), which predicts future errors to reduce overshoot and oscillations. The PID controller was tuned to minimize tracking error and oscillations.

5 Results and Discussion

5.1 Knee exoskeleton tracking performance under PID control

This section analyzes the performance of the PID controller in tracking the desired knee joint angle. The PID gains were tuned iteratively to minimize tracking error. Figures 5, 6, and 7 shows desired and actual knee joint angles, angular velocities, positions of the distal end of the shank frame (derived using forward kinematics) and knee torque along with the resulting tracking errors for best tuned PID gains ($K_p = 100$, $K_i = 10$, $K_d = 180$). The actual knee joint trajectory (red) closely follows the desired trajectory (blue), demonstrating excellent tracking performance over the complete gait cycle. The technical feasibility of the PID controller was computed using three performance metrics: Mean Absolute Error (MAE), Root Mean Square Error (RMSE), and Integral of Absolute Error (IAE). MAE measures the average difference between the actual and desired knee joint angles over the complete gait cycle. Similarly, RMSE measures deviation from the desired knee joint angle, but it penalizes higher deviations more strongly than MAE. IAE provides cumulative deviation throughout the gait cycle.

$$MAE = \frac{1}{N} \sum_{i=1}^N |\theta_d(i) - \hat{\theta}(i)| \quad (11)$$

$$RMSE = \sqrt{\frac{1}{N} \sum_{i=1}^N (\theta_d(i) - \hat{\theta}(i))^2} \quad (12)$$

$$\text{IAE} = \sum_{i=1}^N |\theta_d(i) - \hat{\theta}(i)| \Delta t \quad (13)$$

where θ_d is the desired knee angle and $\hat{\theta}$ is the actual joint angle.

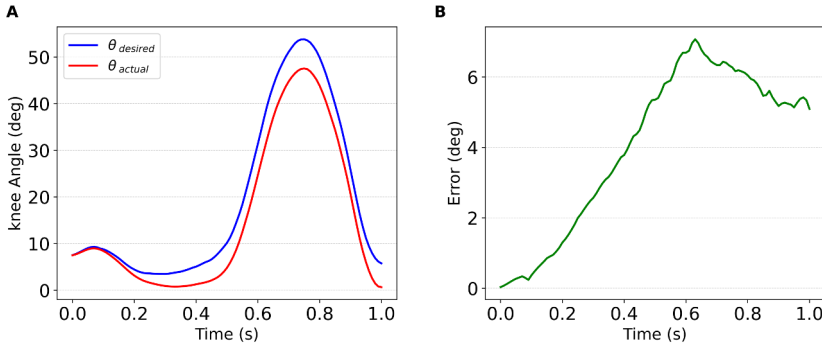


Figure 5. Comparison of desired and actual knee joint angles over the complete gait cycle. (A) Desired vs actual knee angles. (B) Corresponding tracking error.

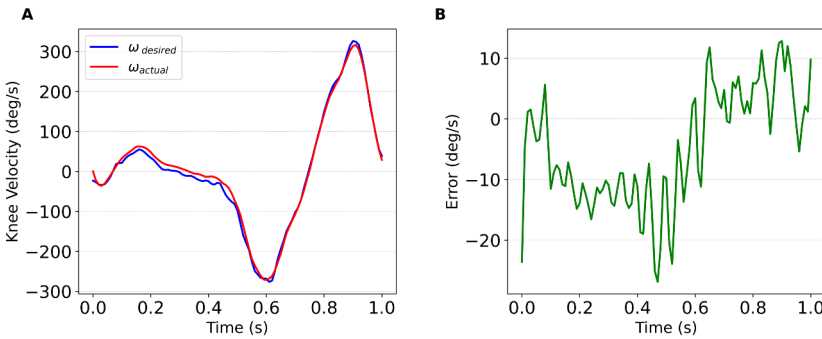


Figure 6. Comparison of desired and actual knee joint angular velocity over the complete gait cycle. (A) Desired vs actual knee velocity. (B) Corresponding tracking error.

The PID controller with best tuned gains yields excellent trajectory tracking, with a mean absolute error (MAE) of 4.05° , a root mean square error (RMSE) of 4.65° , and an integral of absolute error (IAE) of $4.07^\circ \cdot s$. The maximum absolute position error observed at the distal end of the shank frame is 2.2 cm along the x-axis and 4.2 cm along the y-axis. The dynamic analysis reveals that the peak torque requirement is 34.76 Nm, occurring during the terminal stance phase (50-60% of the gait cycle). Based on peak torque requirement, a BLDC motor with a maximum rated torque of 41 Nm can be selected. Following this, a motor with a 1.8 Nm torque is selected, coupled with a gearbox of a 22.7:1 reduction ratio, from a local vendor [19]. Since the combined weight of the motor-gearbox assembly is 1.7 kg, the total weight of the knee exoskeleton, including the motor, becomes 3.5 kg per leg.

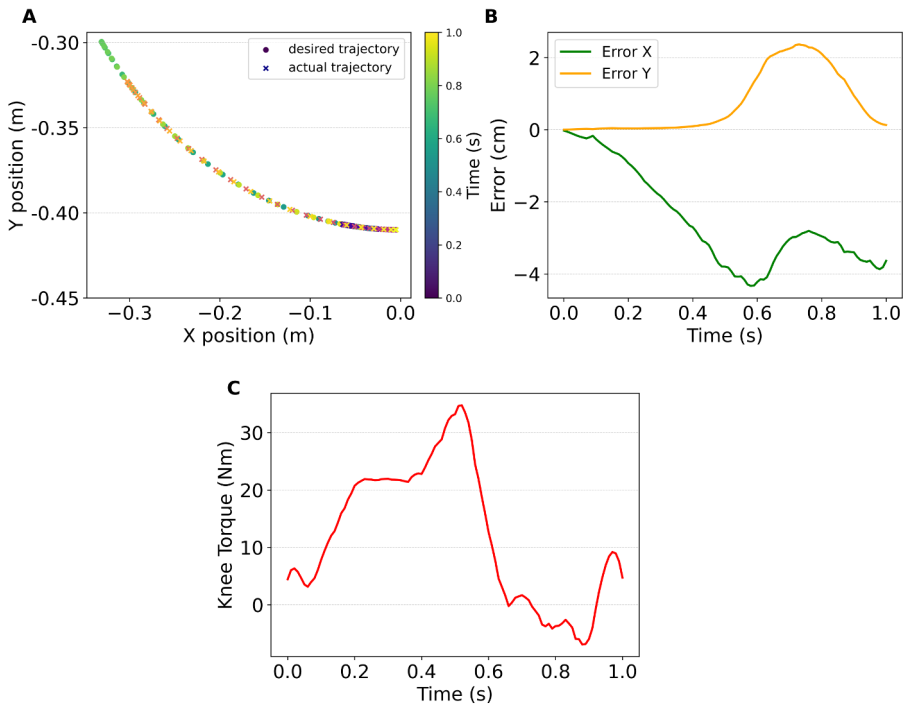


Figure 7. Comparison of desired and actual trajectories of the distal end of the shank during one gait cycle. (A) Desired and actual end-point trajectories. (B) Tracking errors in the X and Y directions. (C) Corresponding knee joint torque profile.

5.2 Effect of PID gain variation on knee angle tracking

The performance of the knee exoskeleton under different PID controller gains was evaluated in terms of joint angle tracking, tracking error, and required torque. Figure 8 shows the comparison between the desired and actual knee joint angles for four sets of PID gains. The four PID gain sets are: PID A ($K_p = 50$, $K_i = 20$, $K_d = 40$), PID B ($K_p = 100$, $K_i = 20$, $K_d = 40$), PID C ($K_p = 100$, $K_i = 20$, $K_d = 120$), and PID D ($K_p = 100$, $K_i = 10$, $K_d = 180$). It can be observed that increasing the proportional gain (K_p) and derivative gain (K_d) improves the tracking performance and reduces peak error, resulting in the actual trajectory following the desired trajectory more closely. MAE, RMSE, and IAE in knee angle tracking for four different sets of PID gains are shown in Table 1. Figure 9 shows the knee joint velocities and torque profiles for the different PID gains. MAE decreases from 13.86° (PID A) to 4.05° (PID D) on increasing proportional and derivative gains. RMSE decreases from 15.83° (PID A) to 4.65° (PID D) on tuning PID with higher gains. IAE also decreases from $13.93^\circ \cdot s$ (PID A) to $4.07^\circ \cdot s$ (PID D), indicating efficient tracking of the knee joint angle. On tuning PID, all three errors decrease, and the actual knee joint trajectory closely follows the desired trajectory. Moreover, the maximum knee torques for four different sets of PID gains are 28.7, 31.59, 30.53, and 34.76 Nm, respectively.

Overall, the results clearly demonstrate that increasing the proportional and derivative gains significantly enhances the tracking accuracy and stability of the knee exoskeleton. The optimized PID configuration (PID D) achieved the lowest MAE, RMSE, and IAE, with the actual joint trajectory closely matching the desired motion. This indicates that appropriate

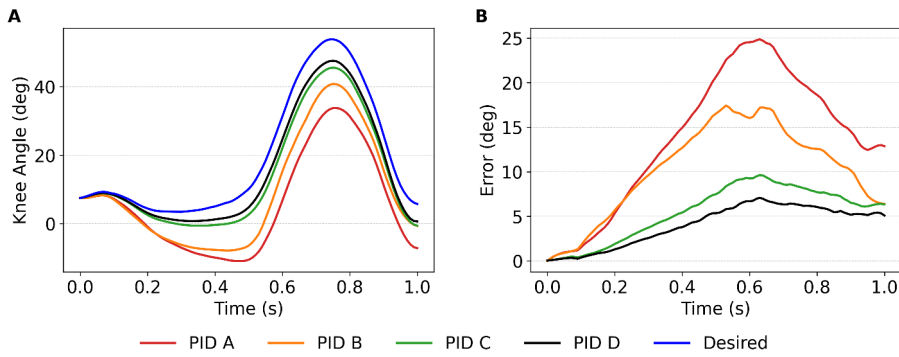


Figure 8. Knee joint angle tracking performance for four PID gain sets. (A) Desired and actual knee joint angles over the complete gait cycle. (B) Tracking errors. The PID parameters are: PID A ($K_p = 50, K_i = 20, K_d = 40$), PID B ($K_p = 100, K_i = 20, K_d = 40$), PID C ($K_p = 100, K_i = 20, K_d = 120$), PID D ($K_p = 100, K_i = 10, K_d = 180$).

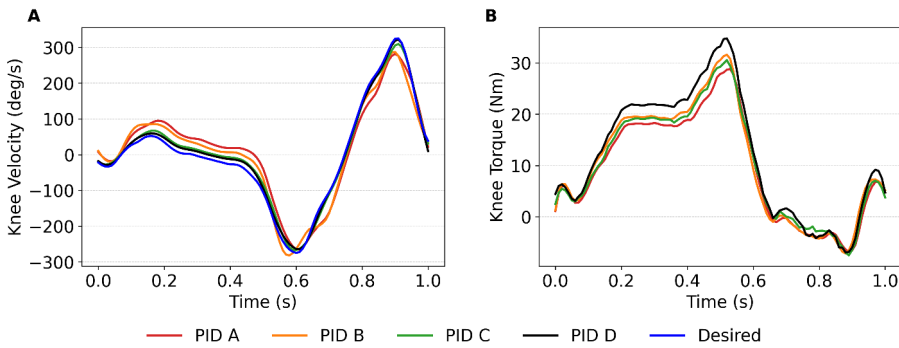


Figure 9. Knee joint velocity and torque profiles corresponding to PID gain sets A–D. (A) Angular velocity trajectories. (B) Corresponding joint torque.

Table 1. Knee joint angle tracking errors for different PID gains

PID Gain	MAE (deg)	RMSE (deg)	IAE (deg·s)
PID A	13.8555	15.8320	13.9298
PID B	10.3013	11.5139	10.3722
PID C	5.4741	6.2628	5.4970
PID D	4.0544	4.6473	4.0693

PID tuning effectively minimizes tracking errors while maintaining smooth torque response, ensuring reliable and precise motion assistance for knee rehabilitation.

5.3 Comparison with existing knee exoskeletons

A comparative assessment of this study was conducted to evaluate the performance of the proposed underwater exoskeleton in comparison to existing exoskeleton literature. Simulation results based on our study yielded a mean absolute error of 4.05° with the optimal PID

gains ($K_p = 100$, $K_i = 10$, $K_d = 180$). Comparing this with other studies, a mean absolute error (MAE) of 4.79° was reported during walking trials for an impedance-controlled land-based system [20]. Relatively higher tracking errors of approximately 10° were observed when employing a zeroing dynamic-based controller subjected to time-varying disturbances [21]. Similarly, the PID-controlled system analyzed by Mefoued and Belkhiat [22] exhibited knee joint angle RMSE values between 4.2° and 5.9° , which are closely aligned with our recorded RMSE of 4.65° . An underwater lower-extremity exoskeleton was also developed in prior work, but it provided assistance to the ankle joint rather than the knee joint as targeted in our study, further highlighting the significance of our system [23]. Collectively, these comparisons indicate that the proposed underwater exoskeleton's performance is competitive with existing terrestrial systems and represents a unique design developed for effective underwater load augmentation.

6 Conclusion

A novel knee exoskeleton design weighing 3.5 kg per leg (including the actuator) has been proposed for load augmentation in underwater conditions. For tracking the desired knee joint trajectory, PID-based position control was implemented in Simscape Multibody, and its performance was evaluated for various gains. Simulation results demonstrate excellent trajectory tracking with the best-tuned PID gains ($K_p = 100$, $K_i = 10$, $K_d = 180$), resulting in a mean absolute error of 4.05° . Dynamic simulations indicated that supporting a 51 kg load under underwater conditions requires a peak knee joint torque of approximately 41 Nm. Based on this, a BLDC motor with a matching torque capacity was selected for the exoskeleton design. Future work will focus on the fabrication and experimental validation of the proposed prototype, followed by human-subject testing to evaluate its effectiveness in reducing metabolic cost during underwater load carriage. Furthermore, modern control schemes, such as disturbance-rejection control, will be explored to improve trajectory tracking under varying hydrodynamic disturbances.

Acknowledgments

This work was supported by the IIT Guwahati Technology Innovation and Development Foundation (IITG TIDF) under grant number TIH/TD/0502, and the authors gratefully acknowledge this support.

References

- [1] Masood, J., Ortiz, J., Fernández, J., Mateos, L.A. and Caldwell, D.G., 2016, June. Mechanical design and analysis of light weight hip joint parallel elastic actuator for industrial exoskeleton. In 2016 6th IEEE international conference on biomedical robotics and biomechatronics (BioRob) (pp. 631-636). IEEE.
- [2] Bortole, M., Venkatakrishnan, A., Zhu, F., Moreno, J.C., Francisco, G.E., Pons, J.L. and Contreras-Vidal, J.L., 2015. The H2 robotic exoskeleton for gait rehabilitation after stroke: early findings from a clinical study. *Journal of neuroengineering and rehabilitation*, 12(1), p.54.
- [3] Narayan, J. and Kumar Dwivedy, S., 2021. Preliminary design and development of a low-cost lower-limb exoskeleton system for paediatric rehabilitation. *Proceedings of the Institution of Mechanical Engineers, Part H: Journal of Engineering in Medicine*, 235(5), pp.530-545.

- [4] Narayan, J., Abbas, M. and Dwivedy, S.K., 2024. Design and validation of a pediatric gait assistance exoskeleton system with fast non-singular terminal sliding mode controller. *Medical Engineering & Physics*, 123, p.104080.
- [5] Cao, W., Chen, C., Wang, D., Wu, X., Chen, L., Xu, T. and Liu, J., 2021. A lower limb exoskeleton with rigid and soft structure for loaded walking assistance. *IEEE Robotics and Automation Letters*, 7(1), pp.454-461.
- [6] Zoss, A. and Kazerooni, H., 2006. Design of an electrically actuated lower extremity exoskeleton. *Advanced Robotics*, 20(9), pp.967-988.
- [7] Fontana, M., Vertechy, R., Marcheschi, S., Salsedo, F. and Bergamasco, M., 2014. The body extender: A full-body exoskeleton for the transport and handling of heavy loads. *IEEE Robotics & Automation Magazine*, 21(4), pp.34-44.
- [8] Fan, W., Dai, Z., Zhang, B., He, L., Pan, M., Yi, J. and Liu, T., 2024. HyExo: A novel quasi-passive hydraulic exoskeleton for load-carrying augmentation. *IEEE/ASME Transactions on Mechatronics*, 30(1), pp.144-155.
- [9] Zhou, Z., Xu, M., Wang, Z., Gao, H., Mai, J. and Wang, Q., 2024, July. Mechatronic Design of a Shank-Free Bilateral Exoskeleton for Loaded Walking. In *2024 IEEE International Conference on Advanced Intelligent Mechatronics (AIM)* (pp. 1398-1403). IEEE.
- [10] Mishra, S., Narayan, J., Nikum, A.K. and Singh, R., 2022. Design and Modeling of a Novel Exoskeleton Suit for Load-Bearing Augmentation. In *Revolutions in Product Design for Healthcare: Advances in Product Design and Design Methods for Healthcare* (pp. 53-74). Singapore: Springer Singapore.
- [11] Xia, H., Zhang, B. and Feng, Y., 2023, July. A conceptual underwater soft exoskeleton for augmenting human breaststroke. In *2023 International Conference on Advanced Robotics and Mechatronics (ICARM)* (pp. 906-911). IEEE.
- [12] Salgado-Gomes-Sagaz, F., Zorrilla-Muñoz, V. and Garcia-Aracil, N., 2024. Rehabilitation technologies by integrating exoskeletons, aquatic therapy, and quantum computing for enhanced patient outcomes. *Sensors*, 24(23), p.7765.
- [13] Birrell, S.A., Hooper, R.H. and Haslam, R.A., 2007. The effect of military load carriage on ground reaction forces. *Gait & posture*, 26(4), pp.611-614.
- [14] Plagenhoef, S., Evans, F.G. and Abdelnour, T., 1983. Anatomical data for analyzing human motion. *Research quarterly for exercise and sport*, 54(2), pp.169-178.
- [15] Davis, J.R., 1993. Aluminum and aluminum alloys. ASM international.
- [16] Barela, A.M., Stolf, S.F. and Duarte, M., 2006. Biomechanical characteristics of adults walking in shallow water and on land. *Journal of Electromyography and Kinesiology*, 16(3), pp.250-256.
- [17] Al-Hayali, N.K., Nacy, S.M., Chiad, J.S. and Hussein, O., 2021. A Mathematical model of the human lower limb during a complete gait cycle and its various phases. *Journal of Mechanical Engineering Research and Developments*, 44(8), pp.392-405.
- [18] Kong, K., Moon, H., Hwang, B., Jeon, D. and Tomizuka, M., 2009, May. Robotic rehabilitation treatments: Realization of aquatic therapy effects in exoskeleton systems. In *2009 IEEE International Conference on Robotics and Automation* (pp. 1923-1928). IEEE.
- [19] Bholanath Precision Engineering Pvt. Ltd., 2025, Products. Available at: <https://bholanath.in/shop/products.html> (Accessed: 06 November 2025).
- [20] Meng, W., Tian, Z., Zhu, C., Ai, Q. and Liu, Q., 2024. Optimized Impedance Control of a Lightweight Gait Rehabilitation Exoskeleton Based on Accurate Knee Joint Torque Estimation. *IEEE Transactions on Medical Robotics and Bionics*.
- [21] Li, Z., Ma, W., Yin, Z. and Guo, H., 2017. Tracking control of time-varying knee exoskeleton disturbed by interaction torque. *ISA transactions*, 71, pp.458-466.

- [22] Mefoued, S. and Belkhat, D.E.C., 2019. A robust control scheme based on sliding mode observer to drive a knee-exoskeleton. *Asian Journal of Control*, 21(1), pp.439-455.
- [23] Wang, Q., Zhou, Z., Zhang, Z., Lou, Y., Zhou, Y., Zhang, S., Chen, W., Mao, C., Wang, Z., Lou, W. and Mai, J., 2020. An underwater lower-extremity soft exoskeleton for breaststroke assistance. *IEEE Transactions on Medical Robotics and Bionics*, 2(3), pp.447-462.